

# LiCS: Navigation using Learned-imitation on Cluttered Space

Joshua Julian Damanik, Jae-Won Jung, Chala Adane Deresa, and Han-Lim Choi

**Abstract**—In this letter, we propose a robust and fast navigation system in a narrow indoor environment for UGV (Unmanned Ground Vehicle) using 2D LiDAR and odometry. We used behavior cloning with Transformer neural network to learn the optimization-based baseline algorithm. We inject Gaussian noise during expert demonstration to increase the robustness of learned policy. We evaluate the performance of LiCS using both simulation and hardware experiments. It outperforms all other baselines in terms of navigation performance and can maintain its robust performance even on highly cluttered environments. During the hardware experiments, LiCS can maintain safe navigation at maximum speed of 1.5 m/s.

**Index Terms**—imitation-learning, indoor navigation, cluttered environment, UGV.

## I. INTRODUCTION

NAVIGATION within cluttered indoor environments poses a substantial challenge for Unmanned Ground Vehicles (UGVs). Ensuring robust and rapid navigation in such cluttered spaces is vital for applications that range from warehouse automation to search and rescue missions. Traditional navigation systems often encounter difficulties in these environments due to tight spaces and numerous obstacles [1], [2].

The recent availability of benchmarking datasets [3], [4] for navigation in cluttered environments has facilitated significant advancements in learning-based navigation systems, particularly through the use of reinforcement learning (RL) [5] and imitation learning (IL) [6]. RL shows promise but can result in unexpected behaviors and requires extensive reward function engineering for effective training [7].

Imitation learning (IL), in contrast, aims to replicate the behavior of an expert, be it a human or optimal control algorithm. This complex task can be simplified into a supervised learning model known as Behavior Cloning (BC). However, BC faces limitations due to its assumption that data in the training dataset are sampled independently of the environment [8]. In practice, actions taken during training influence future states, leading to compounded errors in the learned policy [9].

To mitigate these challenges, techniques like SMILE [9] and DAgger [10] combine BC with sequential online learning to maintain policy performance. Although effective, these methods require ongoing expert interaction during training, which can be resource-intensive. Offline BC, alternatively, emphasizes careful planning of the demonstrations to ensure comprehensive exploration coverage. A key strategy involves

J. J. Damanik, J.-W. Jung, C. A. Deresa, and H.-L. Choi were with the Department of Aerospace Engineering, Korea Advanced Institute of Science and Technology, Daejeon, Republic of Korea. E-mail: (joshuad, jjwon13, czchala99, hanlimc)@kaist.ac.kr.

introducing controlled noise to the input controls, which has been shown to enhance the robustness and generalizability of the policies [11]–[13].

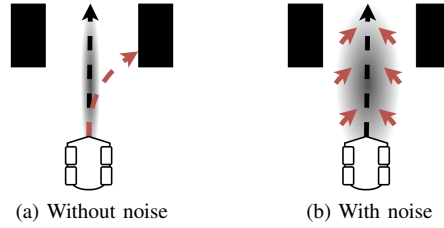


Fig. 1: Demonstrations with exploration noise allow policy to learn how to effectively act on various states

In this letter, we introduce Learned-imitation on Cluttered Space (LiCS), an end-to-end local navigation method to tackle the challenge of navigation in cluttered environments. Our approach utilizes a Transformer-based neural network for imitation learning [14]. During demonstrations, we inject Gaussian noise  $\mathcal{N}(0, \sigma^2)$  to ensure the expert demonstrations cover a broad range of states and induce knowledge of the policy to recover from imminent collision (Fig. 1). This method enables the system to learn and replicate an optimization-based baseline algorithm, adapting it to robustly and rapidly handle cluttered environments. Our proposed method demonstrates a robust capability to navigate a UGV equipped with LiDAR at speeds up to 1.5 m/s through narrow passages, validated in both simulation and real-world experiments.

## II. PROPOSED SYSTEM

The proposed system is a learning-based local planner for a differential robot equipped with LiDAR and odometry sensors. It consists of two main components: a Transformer-based neural network trained through imitation learning and a safety check layer using geometric calculations to ensure the safety of the input control. For a complete system stack, a global planner (e.g., Dijkstra or A\*) is required. Optionally, SLAM can be employed for complex navigation environments and tasks, such as exploration.

### A. Transformer-based neural network

The network used for the imitation learning is depicted in the Fig. 2. Employing both transformer encoder and decoder, the network processes raw LiDAR sensor data and normalized local goal  $\hat{P}$ , derived from a global path obtained from the global planner, to provide outputs of linear and angular

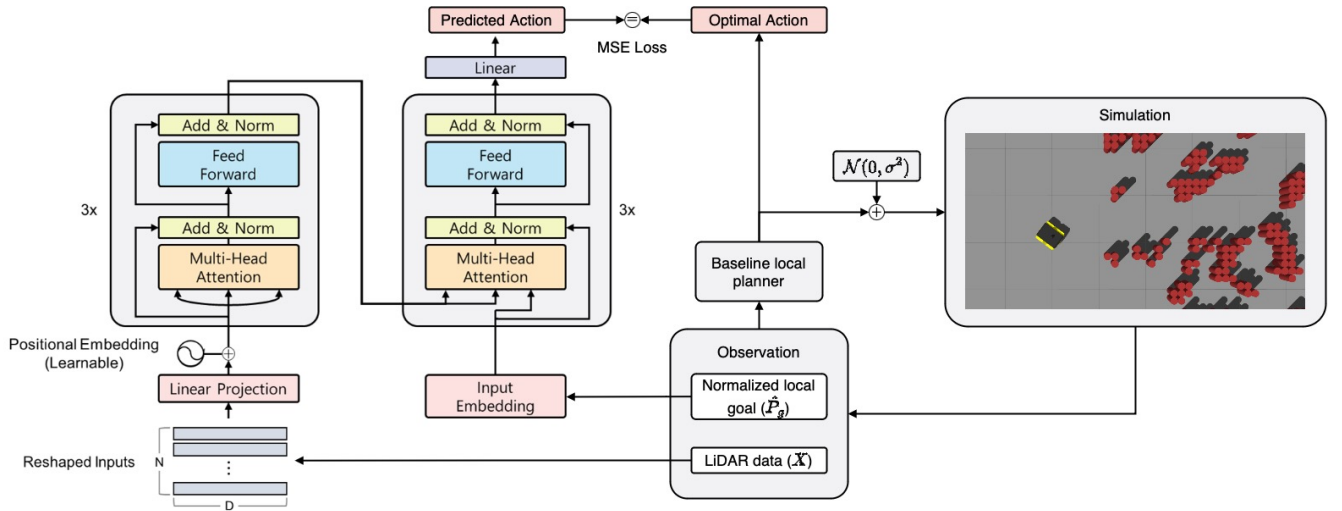


Fig. 2: Training pipeline diagram of the Learned-imitation on Cluttered Space model.

velocity ( $v$  and  $\omega$ ) for the robot. The LiDAR scan data is a vector with length of  $H$  data, and a global path is a list of Cartesian points  $P' = [(x_1, y_1), (x_2, y_2), \dots, (x_k, y_k)]$  from the current robot position towards the global goal point.

To derive the local goal  $P_g$ , points in the global path are transformed from the origin  $O'(0, 0)$  to the robot frame ( $P'_i \rightarrow P_i$ ), selecting the closest point on the global path that has distance  $\|P_i\| \geq L$ ,  $\forall i \in 1, 2, \dots, k$ , where  $L$  is the lookup distance of the robot. The normalized local goal is calculated by dividing the transformed local goal point with its magnitude.

$$P_g = \arg \min_{P_i: \|P_i\| \geq L} \|P_i\| \quad (1)$$

$$\hat{P}_g = \frac{P_g}{\|P_g\|} \quad (2)$$

The transformer encoder's architecture is derived from the ViT (Vision Transformer) [15]. As illustrated in Fig. 2, the encoder inputs raw LiDAR scan data, which consists of distance measurements obtained sequentially increasing laser angles. The input  $X \in \mathbb{R}^{H \times 1}$  is first reshaped into a 2D matrix of patches  $X_p \in \mathbb{R}^{N \times D}$ , where  $N$  is numbers of patches and  $D = H/N$  is the length of the patches. Following reshaping, the input passes through a LiDAR embedding layer consisting of a linear network. After embedding, trainable positional embeddings are added. Unlike the standard ViT where class token row is added during the embedding process, we omit this step as our focus is encoding the observation data for navigation, not classification. The remainder of encoder structure mirrors that of the standard transformer [14].

The transformer decoder processes the normalized local goal as input. During embedding, the the input is passed through a fully connected layer to match the dimension of encoder's output. In contrast to the standard transformer, position encoding and masked multi-head attention layers are omitted due to the non-sequential nature of the input. However, the encoder-decoder attention layers are retained, allowing the network to learn the relationship between the LiDAR scan

and the normalized local goal, which guides the generation of robot commands through a linear transformation.

To facilitate the deployment on embedded systems, we have minimized the number of layers in both the encoder and decoder to three, ensuring the model remains lightweight and operational without requiring GPU (Graphics Processing Unit).

### B. Behavior cloning

Given a dataset  $\mathbb{D}$  consisting of sets of state-action pairs  $\{(s, a^*)\}$  from simulation using an expert controller, our goal is to train a policy  $\pi_\theta(s)$  with parameters  $\theta$  that imitates the expert policy  $\pi^*$ . Behavior cloning (BC) reduces the imitation learning into a supervised learning task aimed at minimizing the following objective:

$$\arg \min_{\theta} \mathbb{E}_{(s, a^*) \sim \mathbb{D}} [l(a^*, \pi_\theta(s))] \quad (3)$$

In our proposed system, we employ an MSE loss function to calculate the discrepancy between the expert action and the learned policy  $l(a^*, \pi_\theta(s))$ . The network, as shown in Fig. 2, is trained using simulation of differential robot model. We deploy the model of cluttered environment for robot navigation as proposed in [3]. During training, exploration noise modeled as Gaussian function with standard deviation  $\sigma$  is added to the output velocity action, modifying the input action in the simulation to include noise rather than the optimal one.

$$v = v^* + \mathcal{N}(0, \sigma^2) \quad (4)$$

$$\omega = \omega^* + \mathcal{N}(0, \sigma^2) \quad (5)$$

Using the LiDAR sensor data  $X$  and normalized local goal  $\hat{P}_g$  as input for the neural network model, and the optimal output velocity action  $(v^*, \omega^*)$  provided by the baseline algorithm as the target value, we trained the proposed network in a supervised manner using MSE loss of the predicted and optimal velocity action (Eq. 3).

### C. Safety check layer

The output of the neural network is often unpredictable, especially in unexplored domains, potentially leading to unsafe behavior and collisions with obstacles. To mitigate this risk, we introduce a safety check layer that takes inputs from observation data (LiDAR or costmap generated by the global planner) and the neural network's output velocity action. The computation is performed in the sensor domain, enabling fast and efficient calculation and allowing real-time supervision of the model output before passing input control into the motor controller.

Movement safety is predicted using geometric calculations [16]. We model the robot into a polygon centered at the middle point along the axle of the robot. While the shape can be arbitrary,  $h$  and  $l$  represents maximum distances between two points along the  $y$ - and  $x$ -axis, respectively. For the sake of simplicity, we assume the robot's shape is a rectangle with dimensions  $l$  and  $h$ .

1) *Linear motion with constant velocity* ( $|v| > 0, \omega = 0$ ): During linear motion, the robot moves forward or backward along the  $x$ -axis relative to its frame of reference, at a constant velocity ( $|v| > 0, \omega = 0$ ). The safety check for linear motion involves determining whether any obstacles lie within a predefined ROI (Region of interest) directly ahead of the robot. This ROI is defined as a rectangular area extending from the front or back of the robot up to a certain distance (maximum observable distance) and covering the width of the robot.

The robot's movement is defined as "unsafe" if there exists a point with coordinate  $(x, y)$  that lies within the ROI, satisfying the following conditions:

$$\begin{cases} xv > 0 \\ |y| \leq h/2 \end{cases} \quad (6)$$

2) *Radial motion with constant velocity* ( $|v| > 0, |\omega| > 0$ ): During radial motion, the robot turns at a constant angular velocity ( $\omega$ ), causing it to move along a circular arc with a turning radius  $R$ . The safety check for radial motion involves determining whether any obstacles lie within a predefined ROI along this arc. The turning radius  $R$  is calculated as the ratio of the linear velocity ( $v$ ) to the angular velocity ( $\omega$ ).

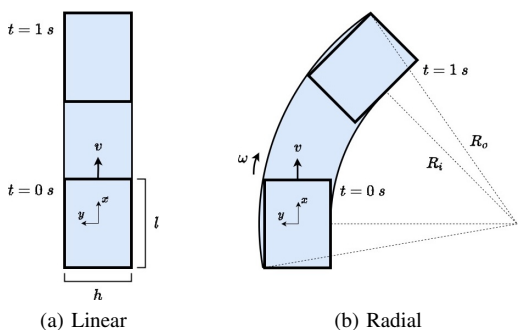


Fig. 3: ROI illustration for safety check layer during linear and radial movement.

Given the arbitrary width of the robot, let  $R_o$  be the outer turning radius and  $R_i$  be the inner turning radius. The ROI is calculated by generating two polygons of the robot at initial and final positions (after  $\Delta t$ ) and connecting the most outer ( $r = R_o$ ) and inner ( $r = R_i$ ) points of the polygons with arcs. The robot's movement is defined as "unsafe" if there exists a point that lies in the ROI. For rectangle robot, we define the outer and inner radii as follows:

$$R_o = \sqrt{(R + h/2)^2 + (l/2)^2} \quad (7)$$

$$R_i = R - h/2 \quad (8)$$

### III. RELATED WORKS

Optimization-based methods have long been foundational in robotics for autonomous navigation, utilizing established algorithms to ensure reliable performance. The Dynamic Window Approach (DWA) [1] emphasizes collision avoidance by dynamically calculating optimal velocity within feasible velocity space, thus reducing computational overhead for quicker responses. Similarly, Elastic Bands (EBand) [2] generate paths through a series of connected points, adjusting these paths via simulated elastic forces to avoid obstacles and minimize travel distance. Another notable optimization approach is the Free-Space Motion Tube (FSMT) technique [16], which defines a robot's maneuvers through adaptive curvature-based motion, allowing efficient navigation in cluttered environments.

On the other hand, learning-based methods leverage advanced machine learning techniques to enhance navigational capabilities. The End-to-End (E2E) algorithm [5] uses Twin Delayed Deep Deterministic Policy Gradient (TD3) to learn navigation policies directly from raw sensor inputs, allowing robots to adapt to diverse environments without predefined rules. Learning from Hallucination (LfH) [17] simulates highly constrained obstacle configurations during training by defining a hallucination function of obstacle configuration. Then the Learning from Learned Hallucination (LfLH) [18] used self-supervised learning to generate motion plan based on the LfH and Inventec [19] extends the LfLH by incorporating a finite state machine to manage recovery behaviors and introduces safety measures to ensure robust navigation in constrained spaces. A hybrid approach is seen in Adaptive Planner Parameter Learning from Reinforcement (APPLR) [20], which combines traditional planning with reinforcement learning. APPLR dynamically adjusts planner parameters at each time step, merging the strengths of classical motion planning with adaptive learning to handle various navigation scenarios effectively.

These diverse approaches highlight the evolution of autonomous navigation techniques, from traditional algorithms ensuring computational efficiency to advanced learning-based methods offering adaptability and robustness, along with hybrid systems that integrate the best of both worlds.

### IV. EXPERIMENT RESULT

This section describes the implementation and evaluation of the proposed system, both in the simulation and through

TABLE I: Performance on benchmark worlds. Bold and square brackets indicate the best and second best performers

Algorithm	Average score	Success (%)	Average Time (s)
Fast-DWA [1]	0.2306	0.8636	25.7320
EBand [2]	0.3256	0.9495	16.7633
APPLR [20]	0.3357	0.8889	16.8034
E2E [5]	0.3712	0.7424	<b>5.1905</b>
LfH [18]	0.4239	0.9141	11.1017
Inventec [19]	0.4242	[0.9899]	13.8181
FSMT [16]	0.4654	<b>1.0000</b>	12.2152
LiCS <sup>a</sup>	0.4455	0.9091	8.5064
LiCS <sup>b</sup>	[0.4874]	0.9747	[7.8487]
LiCS	<b>0.4894</b>	0.9798	8.0182

<sup>a</sup>without safety check and dynamic inflation

<sup>b</sup>without safety check

hardware experiments, using a differential drive UGV model with four wheels and equipped with a 2D LiDAR sensor.

### A. Simulation result

The simulation was performed in Gazebo Classic, utilizing worlds provided by a benchmark dataset [3]. The proposed method generated 300 random worlds with different navigation difficulty metrics derived based on distance to closest obstacle, visibility, dispersion, and tortuosity of every points along the traversable path.

A total 66 test worlds, referred as benchmark worlds, were selected to evaluate our algorithm against the baseline methods. The proposed LiCS algorithm was trained on the remaining environments using the proposed training pipeline. The code for APPLR, EBand, E2E, LfH, and Fast-DWA was sourced from the BARN Challenge public repository <sup>1</sup>, while the code for FSMT and Inventec algorithms was taken from the authors' public repositories <sup>2 3</sup>.

Each algorithm were subjected to three trials in the benchmark environments. Metrics recorded include average score, success rate, and average traversal time  $T$ . The score metric, adapted from [4], incorporated traversal time as follows:

$$Score = \mathbb{1}_{succ} \frac{T^*}{\text{clip}(T, 2T^*, 8T^*)} \quad (9)$$

The optimal traversal time  $T^*$  is calculated from the shortest path length  $L^*$  of each world, as provided by the dataset, divided by the maximum velocity of UGV (2 m/s). Lower traversal times indicate more efficient and agile navigation. The results of these simulations are summarized in Table I.

Our proposed algorithm, LiCS, demonstrated the highest average score, showcasing robust performance across metrics. LiCS achieved a success rate of 97.98%. Although E2E exhibited the shortest average traversal time of 5.19 seconds, it suffered from a lower success rate in comparison. LiCS provided a balanced approach with an average time of 8.02 seconds, effectively combining speed and safety. To provide a clearer visualization, we plotted the average traversal times

<sup>1</sup><https://github.com/Daffan/the-barn-challenge>

<sup>2</sup><https://github.com/romulorl/barn-kul-fm>

<sup>3</sup><https://github.com/inventec-ai-center/inventec-team-barn-challenge-2023>

TABLE II: Performance on 16 most challenging worlds

Algorithm	Average score	Success (%)	Average Time (s)
Fast-DWA [1]	0.1010	0.5210	36.2100
APPLR [20]	0.1151	0.4792	31.65
E2E [5]	0.1250	0.25	<b>5.6100</b>
LfH [17]	0.2142	0.5210	14.5500
EBand [2]	0.2194	0.6875	19.54
Inventec [19]	0.2932	<b>0.9375</b>	21.5000
FSMT [16]	0.3831	0.8750	14.0878
LiCS <sup>a</sup>	0.3167	0.6458	8.9144
LiCS <sup>b</sup>	<b>0.4583</b>	[0.9167]	8.4039
LiCS	[0.4162]	0.8438	[7.8345]

<sup>a</sup>without safety check and dynamic inflation

<sup>b</sup>without safety check

(over three trials) for each algorithm and the average score by grouping test worlds into 6 bins in Fig. 4

To evaluate the performance limits of these algorithms, we selected 16 of most challenging worlds from the BARN dataset, where most algorithms had previously scored the lowest. This selection aimed to rigorously test the robustness and adaptability of each algorithm under difficult navigation scenarios. Each algorithm was tested over three iterations in these hard worlds. The results of this evaluation are summarized in Table II.

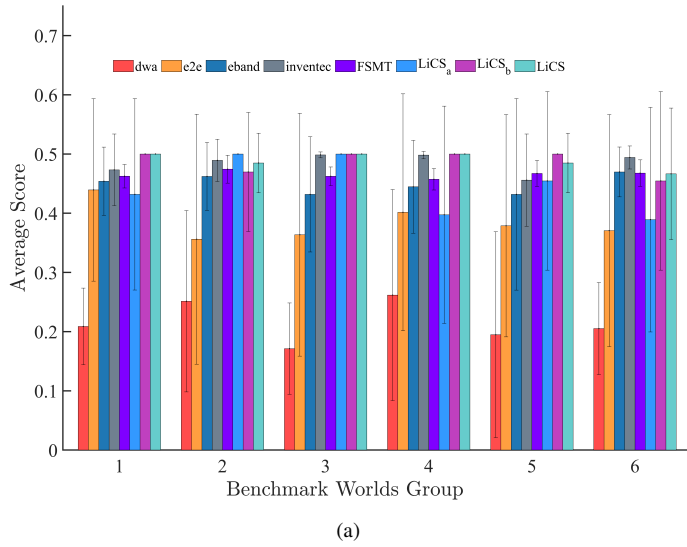
In these challenging environments, LiCS consistently outperformed the other algorithms, achieving the highest and second highest average scores and still maintaining high success rate. Although E2E had the shortest average traversal time of 5.61 seconds, LiCS demonstrated a balanced performance with an average time of 7.83 seconds.

Through the process of comparing the performance of LiCS with other algorithms, it becomes evident that our proposed algorithm strikes a balance between high success rates, low collision rates, and reasonable completion times. Unlike some algorithms that excel in one aspect but lag in others (e.g., E2E's low collision rate but poor success rate in hard worlds), LiCS maintains a strong overall performance, making it suitable for a wide range of real-world applications.

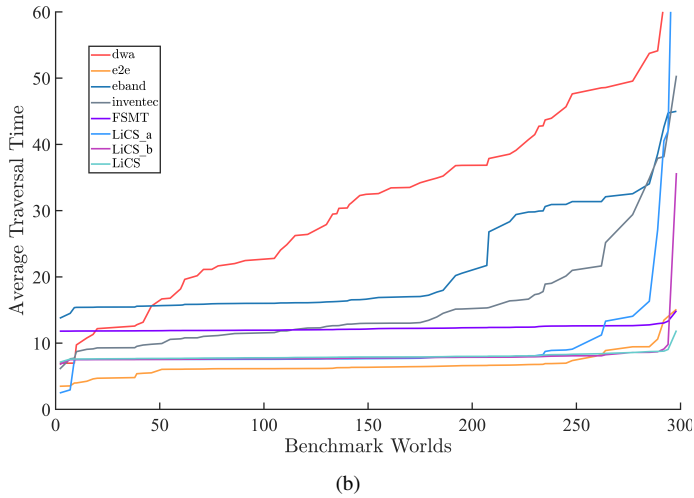
### B. Hardware Experiment Result

The robot used for hardware experiment is identical to the one used in simulation experiment, hence allowing the performance comparison between the simulation and real implementation (sim-to-real). The algorithm was deployed in Jackal robot equipped with Hokuyo UST-20LX LiDAR and Intel i3 CPU controller, operating without any GPU support.

We conducted tests on three tracks constructed from card boards, each offering different navigation difficulties. The first track was the easiest and the third track was the most difficult. Minimal fine-tuning was applied to the algorithm post-simulation. The identical neural model trained in the simulation was used for the hardware experiments. However the LiDAR sensor differed in resolution between the simulation ( $720 \times 1$ ) and real hardware setups ( $1081 \times 1$ ). To overcome this discrepancy, we scale down the hardware sensor data size by linearly sampling of the real sensor data to match the required model input size. Additional adjustments were made to the



(a)



(b)

Fig. 4: (a) Average scores of algorithms for each benchmark worlds group. (b) Average traversal times across benchmark worlds.

TABLE III: Hardware Experiment Results

Trial	Track 1 (s)	Track 2 (s)	Track 3 (s)
1	32	37	X
2	31	37	X
3	32	40	X
4	27	29	X
5	30	32	X
Average	30.4	35	X

velocity settings and the inflation radius of the global cost map to optimize the performance.

The results of the hardware experiments are presented in Table III. The table lists traversal times for each trial, with "X" indicating a failure to complete the track caused by collision. Our algorithm successfully navigated track 1 and 2 but failed on track 3. The difficulty increased progressively across the tracks. Particularly, track 3 featured narrow path requiring sharp turns, which proved too challenging. During the experiments, several parameters were adjusted, including

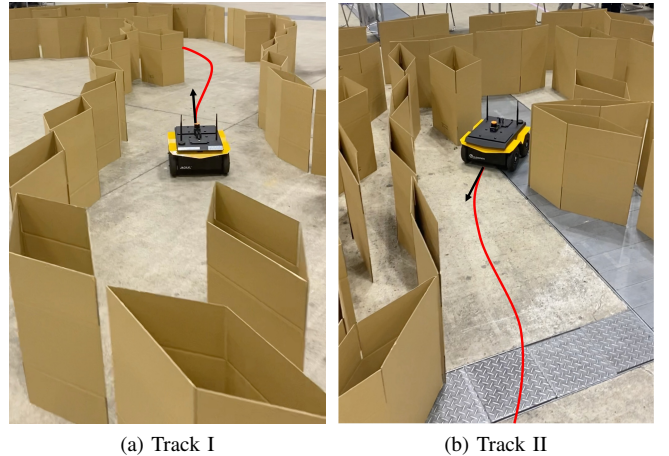


Fig. 5: Robots navigating the first and second tracks, delineated by cardboard boundaries. The red lines indicate the robot's future trajectory, and the black arrows show the direction of movement.

maximum linear velocity, angular velocity, and inflation radius. For the first three trials on tracks 1 and 2, the maximum linear and angular velocities were set to 1.0 m/s and 1.0 rad/s, respectively. In subsequent trials, the maximum linear velocity was increased to 1.5 m/s, but the optimal performance was achieved at 1.3 m/s. At higher velocities, the robot moved too aggressively, necessitating frequent corrective maneuvers, which ultimately increased traversal times. On track 3, the robot frequently collided with obstacles or became stuck at tight corners due to the demanding navigation requirements.

## V. CONCLUSION

In this study, we introduced the Learned-imitation on Cluttered Space (LiCS) algorithm, a novel imitation learning-based approach for navigating Unmanned Ground Vehicles (UGVs) through complex, cluttered indoor spaces. This approach utilizes a Transformer-based neural network and combining behavior cloning with robust safety checks. LiCS was designed to optimize navigation by learning from expert demonstrations while adapting to dynamic and unpredictable conditions. It was trained under noisy conditions to generalize across various scenarios. The safety layer integrated into LiCS effectively mitigated potential hazards, preventing collisions and ensuring stable operation under diverse conditions.

The simulation result demonstrated that LiCS provides a significant improvement over baseline methods. It achieved the lowest average traversal time with high success rate, especially in challenging environments characterized by tight spaces. The hardware experiments further validated the simulation results, with LiCS performing reliably on real robots. Although it encountered difficulties in the most challenging track, which highlighted potential limitations in real-world sensor discrepancies and dynamic responses, the overall success in simpler tracks confirmed its practical utility and effectiveness.

This study's findings suggest that the LiCS algorithm represents a promising advancement in the field of autonomous

navigation for UGVs, particularly in scenarios where traditional methods struggle.

#### ACKNOWLEDGMENT

This work was supported by Unmanned Vehicles Core Technology Research and Development Program through the National Research Foundation of Korea (NRF), Unmanned Vehicle Advanced Research Center (UVARC) funded by the Ministry of Science and ICT (MSIT), the Republic of Korea (#2020M3C1C1A0108237512).

#### REFERENCES

- [1] D. Fox, W. Burgard, and S. Thrun, “The dynamic window approach to collision avoidance,” *IEEE Robotics & Automation Magazine*, vol. 4, no. 1, pp. 23–33, 1997.
- [2] S. Quinlan and O. Khatib, “Elastic bands: Connecting path planning and control,” in *[1993] Proceedings IEEE International Conference on Robotics and Automation*. IEEE, 1993, pp. 802–807.
- [3] D. Perille, A. Truong, X. Xiao, and P. Stone, “Benchmarking Metric Ground Navigation,” Nov. 2020, arXiv:2008.13315 [cs, eess]. [Online]. Available: <http://arxiv.org/abs/2008.13315>
- [4] F. Xia, W. B. Shen, C. Li, P. Kasimbeg, M. E. Tchapmi, A. Toshev, R. Martin-Martin, and S. Savarese, “Interactive Gibson Benchmark: A Benchmark for Interactive Navigation in Cluttered Environments,” *IEEE Robotics and Automation Letters*, vol. 5, no. 2, pp. 713–720, Apr. 2020. [Online]. Available: <https://ieeexplore.ieee.org/document/8954627/>
- [5] Z. Xu, B. Liu, X. Xiao, A. Nair, and P. Stone, “Benchmarking reinforcement learning techniques for autonomous navigation,” in *2023 IEEE International Conference on Robotics and Automation (ICRA)*. IEEE, 2023, pp. 9224–9230.
- [6] J. Zhang and K. Cho, “Query-Efficient Imitation Learning for End-to-End Autonomous Driving,” May 2016, arXiv:1605.06450 [cs]. [Online]. Available: <http://arxiv.org/abs/1605.06450>
- [7] Y. Li, “Deep Reinforcement Learning: An Overview,” Nov. 2018, arXiv:1701.07274 [cs]. [Online]. Available: <http://arxiv.org/abs/1701.07274>
- [8] A. Beygelzimer, V. Dani, T. Hayes, J. Langford, and B. Zadrozny, “Error limiting reductions between classification tasks,” in *Proceedings of the 22nd international conference on Machine learning - ICML '05*. Bonn, Germany: ACM Press, 2005, pp. 49–56. [Online]. Available: <http://portal.acm.org/citation.cfm?doid=1102351.1102358>
- [9] S. Ross and J. A. Bagnell, “Efficient Reductions for Imitation Learning,” 2010.
- [10] S. Ross, G. J. Gordon, and J. A. Bagnell, “A Reduction of Imitation Learning and Structured Prediction to No-Regret Online Learning,” Mar. 2011, arXiv:1011.0686 [cs, stat]. [Online]. Available: <http://arxiv.org/abs/1011.0686>
- [11] M. Green and J. B. Moore, “Persistence of excitation in linear systems,” *Systems & Control Letters*, vol. 7, no. 5, pp. 351–360, Sep. 1986. [Online]. Available: <https://linkinghub.elsevier.com/retrieve/pii/0167691186900526>
- [12] M. Laskey, J. Lee, R. Fox, A. Dragan, and K. Goldberg, “DART: Noise Injection for Robust Imitation Learning,” 2017.
- [13] L. Ke, J. Wang, T. Bhattacharjee, B. Boots, and S. Srinivasa, “Grasping with Chopsticks: Combating Covariate Shift in Model-free Imitation Learning for Fine Manipulation,” in *2021 IEEE International Conference on Robotics and Automation (ICRA)*. Xi'an, China: IEEE, May 2021, pp. 6185–6191. [Online]. Available: <https://ieeexplore.ieee.org/document/9561662/>
- [14] A. Vaswani, N. Shazeer, N. Parmar, J. Uszkoreit, L. Jones, A. N. Gomez, Ł. Kaiser, and I. Polosukhin, “Attention is all you need,” *Advances in neural information processing systems*, vol. 30, 2017.
- [15] A. Dosovitskiy, L. Beyer, A. Kolesnikov, D. Weissenborn, X. Zhai, T. Unterthiner, M. Dehghani, M. Minderer, G. Heigold, S. Gelly, J. Uszkoreit, and N. Houlsby, “An Image is Worth 16x16 Words: Transformers for Image Recognition at Scale,” Jun. 2021, arXiv:2010.11929 [cs]. [Online]. Available: <http://arxiv.org/abs/2010.11929>
- [16] R. T. Rodrigues, N. Tsiogkas, N. Huebel, and H. Bruyninckx, “Clutter-resilient autonomous mobile robot navigation with computationally efficient free-space features,” in *The International Symposium of Robotics Research*. Springer, 2022, pp. 522–537.
- [17] X. Xiao, B. Liu, G. Warnell, and P. Stone, “Toward agile maneuvers in highly constrained spaces: Learning from hallucination,” *IEEE Robotics and Automation Letters*, vol. 6, no. 2, pp. 1503–1510, 2021.
- [18] Z. Wang, X. Xiao, A. J. Nettekoven, K. Umasankar, A. Singh, S. Bommakanti, U. Topcu, and P. Stone, “From agile ground to aerial navigation: Learning from learned hallucination,” in *2021 IEEE/RSJ International Conference on Intelligent Robots and Systems (IROS)*. IEEE, 2021, pp. 148–153.
- [19] H. Mandala and G. Christmann, “The barn challenge 2023–autonomous navigation in highly constrained spaces–inventec team,” *arXiv preprint arXiv:2307.14580*, 2023.
- [20] Z. Xu, G. Dhamankar, A. Nair, X. Xiao, G. Warnell, B. Liu, Z. Wang, and P. Stone, “Applr: Adaptive planner parameter learning from reinforcement,” in *2021 IEEE international conference on robotics and automation (ICRA)*. IEEE, 2021, pp. 6086–6092.



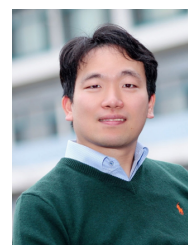
**Joshua Julian Damani** received the B.S. degree in engineering physics from Institut Teknologi Bandung, Indonesia, in 2018, and the M.S. degree in aerospace engineering from the Korea Advanced Institute of Science and Technology (KAIST), Daejeon, South Korea, in 2021, where he is currently pursuing the Ph.D. degree in aerospace engineering KAIST. His current research interests include robotics learning and control, and data mining.



**Jae-Won Jung** received the B.S. degree in mechanical engineering from SungKyunKwan University, Suwon, South Korea in 2018. He is currently pursuing the M.S. degree in aerospace engineering from the Korea Advanced Institute of Science and Technology (KAIST), Daejeon, South Korea. His current research interests include robotics control, and Machine Learning.



**Chala Adane Deresa** received the B.S. degree in aerospace engineering from the Korea Advanced Institute of Science and Technology (KAIST), Daejeon, South Korea, in 2024, where he is currently pursuing the M.S. degree in aerospace engineering. His current research interests include robotics estimation and control, and spacecraft autonomy.



**Han-Lim Choi** (Senior Member, IEEE) received the B.S. and M.S. degrees in aerospace engineering from the Korea Advanced Institute of Science and Technology (KAIST), Daejeon, South Korea, in 2000 and 2002, respectively, and the Ph.D. degree in aeronautics and astronautics from the Massachusetts Institute of Technology (MIT), Cambridge, MA, USA, in 2009. Then, he studied at MIT as a Postdoctoral Associate until he joined KAIST, in 2010. He is currently a Professor of aerospace engineering at KAIST. His current research interests include estimation and control for sensor networks and decision making for multi-agent systems. He was a recipient of the Automatic Applications Prize, in 2011 (together with Dr. Jonathan P. How).